

# Three-dimensional finite element analysis simulations of the fused deposition modelling process

Y Zhang and Y K Chou\*

Mechanical Engineering Department, The University of Alabama, Tuscaloosa, Alabama, USA

*The manuscript was received on 13 February 2006 and was accepted after revision for publication on 1 June 2006.*

DOI: 10.1243/09544054JEM572

**Abstract:** Fused deposition modelling (FDM) is a layer-manufacturing technology that has been widely used for rapid prototyping applications in product design and development. Owing to the intensive energy, rapid cooling, and phase changes, parts made by FDM and other layer-manufacturing processes deviate from the designed geometry, and some require laborious post-processing. Most severe form inaccuracies such as curl, warping, and delamination are attributed to the residual stress accumulations during prototype fabrications.

This study investigates the FDM process, which consists of complicated heat and mass transfer phenomena coupled with mechanical loading and phase changes. A finite element analysis model using element activations has been developed to simulate the mechanical and thermal phenomena in FDM and further used for residual stress and part distortion simulations. The model has also been used to study the tool-path effects on the FDM process. Tool-path patterns affect the residual stresses in not only the magnitude but also the distribution which shows stress concentrations aligned with the primary direction of the tool path. Measured prototypes from the experiment show that the part distortion centre shifts distinctly owing to different tool-path patterns, which is consistent with the residual stress characteristics in the simulations. From the simulations, it is also shown that the short-raster tool path results in higher residual stresses, and thus possibly larger distortions, than the long-raster and alternate-raster patterns, both having similar stress distributions and distortion features.

**Keywords:** fused deposition modelling, finite element analysis, layer manufacturing, part distortion, residual stress

## 1 INTRODUCTION

Layer manufacturing (LM) represents a spectrum of material-processing technologies that produce physical parts directly from three-dimensional solid models, electronic files using computer-aided design (CAD) software, by incrementally and selectively depositing and bonding materials from a source on to a substrate. LM systems read electronically discretized converted CAD surface-model slices and automatically fabricate successive thin layers of the material. To date, LM systems have become common tools for product design and development in various industries ranging from automotive to

medical hardware. Typical LM applications include concept models, fit, and functional testing. More recently, LM systems have also been explored to make tooling and functional parts.

The main differences between various LM processes are the deposition methods and the materials used. For instance, stereolithography apparatus (SLA) systems use an ultraviolet laser to cure liquid polymers into solid resins, selective laser sintering (SLS) also uses laser beams, but to sinter heat-fusible powders, and fused deposition modelling (FDM) extrudes and deposits fused thermoplastics, etc. In addition, new processes have been developed to advance LM. LM processes involve heat and mass transfer, chemical reactions, coupled with mechanical loading and phase changes. Thus, prototypes will mostly depart from the design specifications. Many studies have concerned prototype accuracy.

\*Corresponding author: Mechanical Engineering Department, The University of Alabama, 290 Hardaway Hall, 7th Avenue, Tuscaloosa, Alabama 35487, USA. email: kchou@eng.ua.edu

For example, Qiu and Langrana [1] and Qiu *et al.* [2] studied the tool-path effects on FDM and proposed an algorithm to match the tool path with the extrusion speed, thereby eliminating voids and correcting overfill and underfill defects. Sabourin *et al.* [3] proposed adaptive slicing, according to the surface features, to minimize the staircase effect on accuracy of the part.

FDM is one of the most widely used LM systems because of its inexpensive machinery and durable part materials, e.g. acrylonitrile-butadiene-styrene (ABS). FDM uses two cartridges to supply the part materials and support materials (for overhang structures), which are heated to a semimolten state and then extruded as an ultra-thin semiliquid thermoplastic filament. While the extrusion nozzle is moving according to the tool path defined by part cross-sectional boundaries, the material is deposited on top of the previous layer, and heat dissipation by conduction and force convection causes the material to solidify with the surrounding filaments. The bonding processing encompasses the local remelting of the previously solidified material and diffusion [4, 5]. However, the remelting and rapid cooling may aggravate non-uniform thermal gradients, which generate residual stresses responsible for the part distortions.

Among various geometric errors in LM, residual-stress-induced distortion is one of the most severe conditions. Mahesh *et al.* [6] used a benchmark part to evaluate the performance of almost all LM processes. The measurement results of several tolerance values such as flatness and symmetry were compared, and it was noted that warpage and delamination caused by residual stresses are prominent. Several studies have been conducted to model residual stresses in LM processes; however, few references can be found regarding the residual stresses in FDM. Bugada *et al.* [7] modelled the mechanical aspect in SLA using a finite element analysis (FEA) to study the influence of different constructive and numerical parameters in the curl distortion caused by the shrinkage of the photopolymer. The curl distortion was found to increase with the magnitude of the volumetric shrinkage, and to decrease when the layer thickness increases. Sonmez and Hahn [8] developed thermomechanical models for the laminated-object-manufacturing (LOM) process, correlating process parameters with temperature and stress distributions in the laminates during fabrications. These workers suggested that a large roller diameter and a slower roller speed are favourable for bonding because of a larger roller-paper contact area and longer contact time. Dalgarno *et al.* [9] conducted structural analyses using a finite element method to model the development of the part curling in selective laser sintering. It was reported that sintering the first two layers twice to relieve the

strain developed in these layers would significantly reduce the curling level. Chin *et al.* [10] developed a one-dimensional thermomechanical model to predict the residual stress built up because of successive depositions of superheated molten metals in the shape-deposition-manufacturing (SDM) process. By changing the deposition rate, these researchers studied the effect of succeeding layers on the existing materials and the effect of localized preheating. The same research group [11, 12] further developed thermomechanical models of the deposited layers, droplet columns, and adjacent droplets in SDM. While the localized substrate preheating method was proved not to be effective, process-induced preheating was effective in reducing thermal gradients and residual stresses. Nickel *et al.* [13] developed a three-dimensional FEA model and studied the effect of deposition patterns on the resulting stresses and deflections in SDM. A raster pattern with the trajectory normal to the part's long axis is shown to produce least deflections. Ong [14] analysed the residual stress of thermally deposited polymers in SDM. It was found that polymer depositions show more directionality of warping than the metal deposition. Finnie *et al.* [15] modelled the process of laser metal forming (LMF) and concluded that residual stresses in LMF may be changed from tension to compression by preheating the metal pieces. Beuth and Narayan [16] used FEA to study the residual-stress-induced delamination in multi-layer depositions. The delamination phenomenon was modelled as an interfacial fracture problem. The delamination-energy release rate calculated from the residual stress model can be used to identify critical interfaces where debonding most probably occurs.

Although a few three-dimensional models have been used, most of the above researchers used two-dimensional models for FEA studies of LM processes, which do not consider the geometric change during the LM process. In FDM, the dominant heat transfer mode is conduction and convection, and thus the model geometric change must be included. This study uses FEA to simulate the deposition process of FDM by controlling element activations that participate in the involved mechanical and thermal processes with the residual stress distributions and part distortions studied. The effects of the tool-path pattern on residual stresses and distortion shape in the parts are also investigated.

## 2 FINITE ELEMENT ANALYSIS

FDM is an 'additive' process, during which the volume of the part continuously changes. To simulate the continuous deposition process, the 'element activation-deactivation' function in ANSYS

was used. The element type chosen was for coupled thermomechanical analysis. Since there is no element type in ANSYS that can comply with the above two requirements and yet support the viscoelastic properties (for the semiliquid state) simultaneously, solid structural elements were used in the current phase of the study. The material newly extruded was assumed to be fully in contact with the existing materials around, neglecting the minute gaps between the extruded filaments.

The simulation was conducted in a stepwise thermomechanical manner. After the model was set up and meshed, all the elements were deactivated. When an element is activated, the transient thermal analysis is started with the current temperature distributions as in the initial condition. The calculation of this step continued for an interval of extruding one element of the material. The resulted temperature distribution is then used as the load for the mechanical analysis, which calculates the displacement at each node. Next the next element is activated and the temperature analysis is started again with the convection surfaces updated. Once all the elements have been activated, the calculation is continued until the whole model reaches a thermal equilibrium with the environment.

The governing equation of thermal energy conservation is three-dimensional transient heat conduction with heat generation from the phase changes (enthalpy change) and is given by

$$\frac{\partial(\rho c_p T)}{\partial t} = \nabla \cdot \lambda \nabla T + q \quad (1)$$

where

$\nabla T$  = spatial gradient of the temperature  
 $\rho$  = density  
 $c_p$  = specific heat  
 $\lambda$  = thermal conductivity  
 $q$  = heat generation rate

The energy associated with the phase change is approximated as

$$H = \int \rho c_p(T) dT \quad (2)$$

where

$H$  = enthalpy

The governing equations for mechanical analysis, which are obtained from the stress equilibrium with thermal strain included, given by a thermal expansion coefficient and a reference temperature, are

$$\begin{aligned} \frac{\partial \sigma_x}{\partial x} + \frac{\partial \tau_{yx}}{\partial y} + \frac{\partial \tau_{zx}}{\partial z} &= 0 \\ \frac{\partial \tau_{xy}}{\partial x} + \frac{\partial \sigma_y}{\partial y} + \frac{\partial \tau_{zy}}{\partial z} &= 0 \\ \frac{\partial \tau_{xz}}{\partial x} + \frac{\partial \tau_{yz}}{\partial y} + \frac{\partial \sigma_z}{\partial z} &= 0 \end{aligned} \quad (3)$$

The thermal strain is

$$\varepsilon = \alpha(T - T_{\text{ref}}) \quad (4)$$

where

$\alpha$  = coefficient of thermal expansion  
 $T_{\text{ref}}$  = reference temperature

In the thermal analysis, the temperature at the bottom surface of the part, which is in contact with the platform is set to be constant according to

$$T = T^* \quad (5)$$

where

$T^*$  plate temperature

The boundary conditions of other outer surfaces are convection with a heat convection coefficient and the chamber temperature according to

$$Q = h(T - T_{\text{amb}}) \quad (6)$$

where

$h$  = heat convection coefficient  
 $T_{\text{amb}}$  = chamber temperature

The heat convection coefficient was estimated to be 86 W/m<sup>2</sup> K according to forced-convection analysis [17], with 20 m/s parallel air flow at 75 °C [17]. In the mechanical analysis, the bottom surface of the part was fully constrained from any displacement. In the thermal analysis, the initial temperature of newly activated elements was 280 °C (the extrusion head temperature). For other elements, the initial temperature is obtained from the result of the previous thermal analysis step. In the mechanical analysis, for newly activated elements, the initial displacement is zero. For other elements, the result of the previous mechanical analysis is used as the initial condition of the new step. The temperature result of the thermal analysis is used as the load of the corresponding mechanical analysis.

The extrusion head of the FDM machine used (Prodigy Plus from Stratasys Inc.) has a scanning speed of 16 m/s, and the maximum filament width is about 1 mm. The layer thickness chosen was 0.254 mm. To discretize the deposition process, 1 mm × 1 mm × 0.254 mm elements were set as the smallest unit. The corresponding deposition time was about 0.031 s per element. Parts of 40 mm × 10 mm × 1.016 mm thin plates were simulated using 1600 elements with an assigned sequential order. Each simulation needed computational time of about 30–35 h on a 2.8 GHz central processing unit, 2 GB random-access memory personal computer. A high length-to-width aspect ratio (4 to 1) was selected to examine the tool-path pattern effects. The material properties used were those of ABS plastic (Table 1). All the elements were deactivated before the process began. At each time step, an element was activated with the temperature and

**Table 1** Properties of the work material (ABS)

Property	Value
Conductivity (W/m K)	0.19
Specific heat (kJ/kg K)	
At 0 °C	1.62
At 105 °C	1.62
At 130 °C	3
At 280 °C	1.68
Enthalpy (kJ)	
At 0 °C	0
At 105 °C	109
At 130 °C	153
At 280 °C	308
Density (kg/m <sup>3</sup> )	1200
Poisson's ratio	0.4
Thermal expansion coefficient ( $\mu\text{m}/\text{m K}$ )	80
Young's modulus (GPa)	2.4

displacement fields (of all activated elements) analysed in a thermomechanically coupled manner. The elements were activated in the order of their numbering sequence assigned to follow the deposition path. Once all the elements were activated, the final results were then used for a static thermomechanical coupled analysis to simulate the processes of cooling and unloading. First, the ambient temperature for thermal analysis was changed to room temperature to simulate the condition of taking the part from the machine chamber to the laboratory environment. The displacement constraint of the model in mechanical analysis was then discharged to simulate removing the part from the platform.

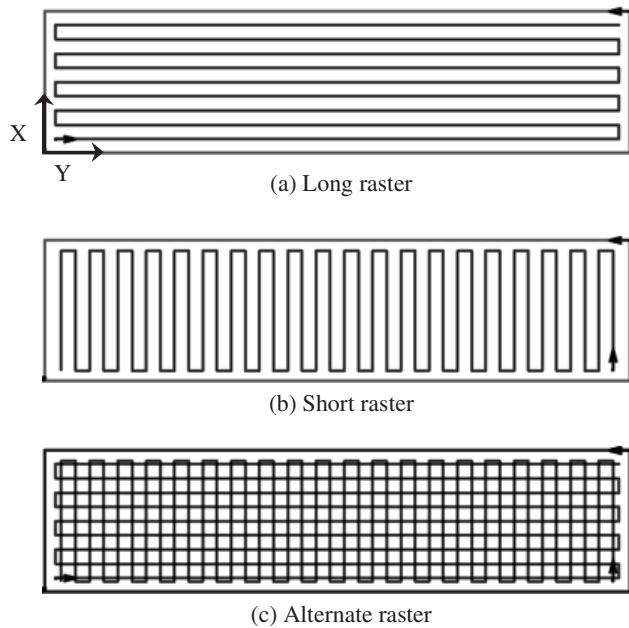
The analysis has been used to investigate the effect of tool-path patterns on residual stresses and part distortions with three cases tested, i.e. long-raster pattern, short-raster pattern, and alternate raster pattern, as in Figs 1(a), (b), and (c), respectively.

### 3 RESULTS AND DISCUSSION

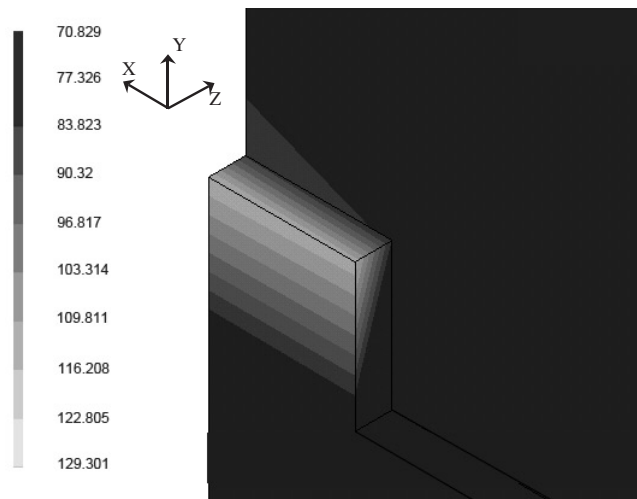
#### 3.1 Element activation demonstration

Figure 2 illustrates an example of the filament deposition simulation, showing temperature distributions immediately after the 1001st element is activated. The tool path used was the alternate-raster pattern, the short-raster pattern being used for the first and third layers. Of the total four layers, each layer has 400 elements, and thus the 1001st element is at the centre-line of the third layer. When the temperature distribution is calculated, the result is shared as the load to analyse the strain and stress distributions (Fig. 3).

Figures 4(a), (b), and (c) show the stress (maximum principal stress) evolution in the part during a series of element activations (801st, 1002nd, and 1156th elements respectively) as in the deposition.



**Fig. 1** Sketches showing the different tool-path patterns tested



**Fig. 2** Temperature distributions ( $^{\circ}\text{C}$ ) when the 1001st element was just activated

The 801st element is the first element activated on the third layer. The second layer has a long-raster pattern, and thus the bottom surface shows the stress concentration pattern caused by the long-raster toolpath, i.e. stresses accumulated along the length side. At each layer, the stress starts to accumulate at the locations of the initial deposition. Thus, around the first line of the tool path, an area of high stresses matching the tool-path pattern can be observed (Fig. 4(a)). In addition, at tool-path turning points, the boundary conditions may cause greater thermal gradients and leave stress accumulation marks that can be seen. The 1002nd element is at around 50 per cent completion of the third layer

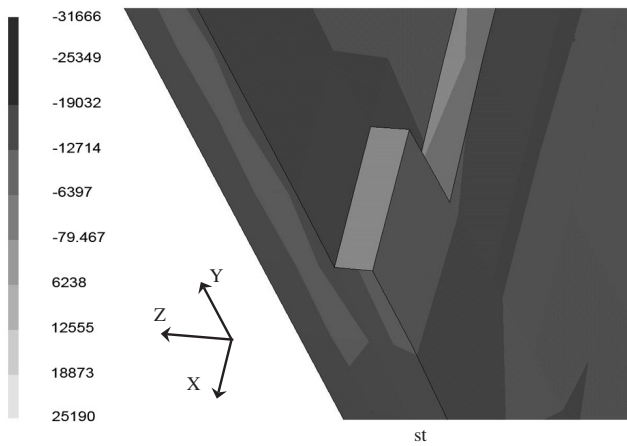
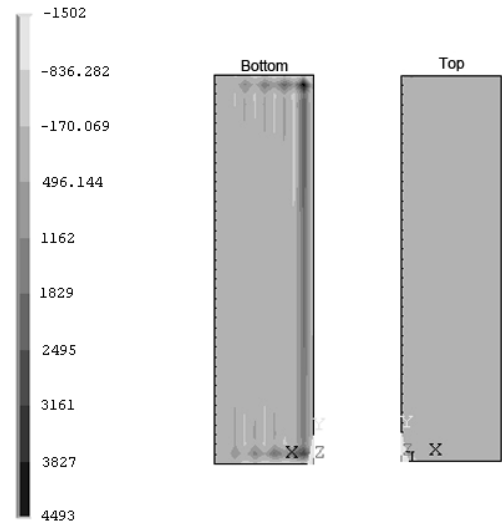


**Fig. 3** Stress distributions (Pa) when the 1001st element was just activated

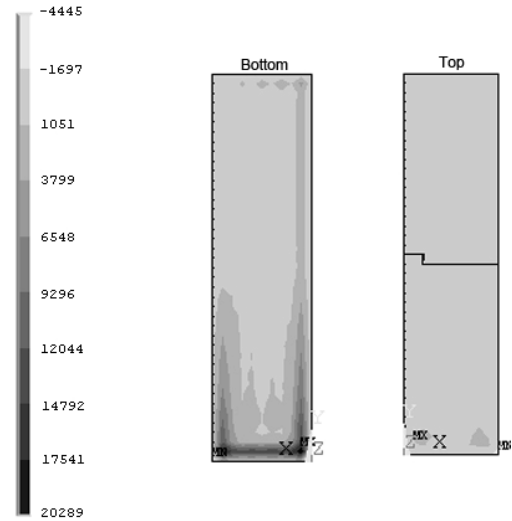
and, as shown, the maximum principal stress contours show half long-raster and half short-raster characteristics. The 1156th element is near the end of the third layer and, at this moment, the residual stress on the bottom surface mostly corresponds to the short-raster pattern with a little residue from the long-raster pattern of the previous layer. The magnitude of the residual stresses increases as expected when the process continues, e.g. a maximum 4.5 kPa at the 801st element and a maximum 28.9 kPa at the 1156th element. This resulted from the number of heating-cooling cycles, and the time interval between the cycles. Figure 5 shows the stress distributions at the completion of each layer deposition. Obvious changes in the stress pattern correspond to the tool-path patterns at different layers. In addition, the results show that stress concentrations are owing to the fixed boundary conditions at the bottom layer.

**3.2 Tool-path pattern effects**

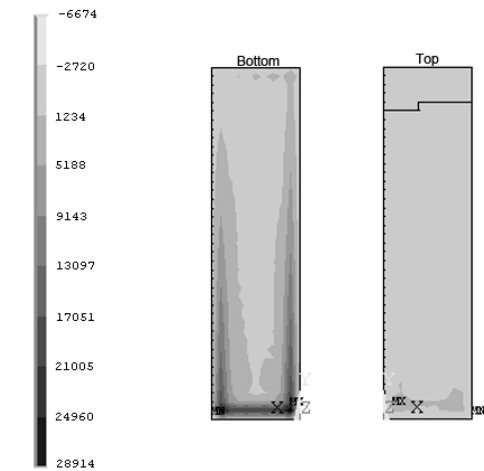
The simulation algorithm was used to evaluate three different tool-path cases: long-raster, short-raster, and alternate-raster patterns. Figure 6 plots, for each toolpath pattern, the residual stresses (maximum principal stress) in the part, after complete depositions. From the plots, the tool-path effect on stress build-up is clearly noted. Firstly, on the stress scale, the long-raster and alternate-raster patterns lead to, both in a close range, smaller residual stresses than the short-raster pattern does. Secondly, the maximum stress zone shifts away from the centre of the part, aligned with the primary moving direction of the tool path, for all three tool-path patterns. During the deposition process, the residual stress is the smallest for the most recently activated elements, while the earliest activated elements



(a) 801<sup>st</sup> element



(b) 1002<sup>nd</sup> element



(c) 1156<sup>th</sup> element

**Fig. 4**  $\sigma_1$  (maximum principal stress) distributions (Pa) during a series of element activations: (a) 801st element; (b) 1002nd element; (c) 1156th element

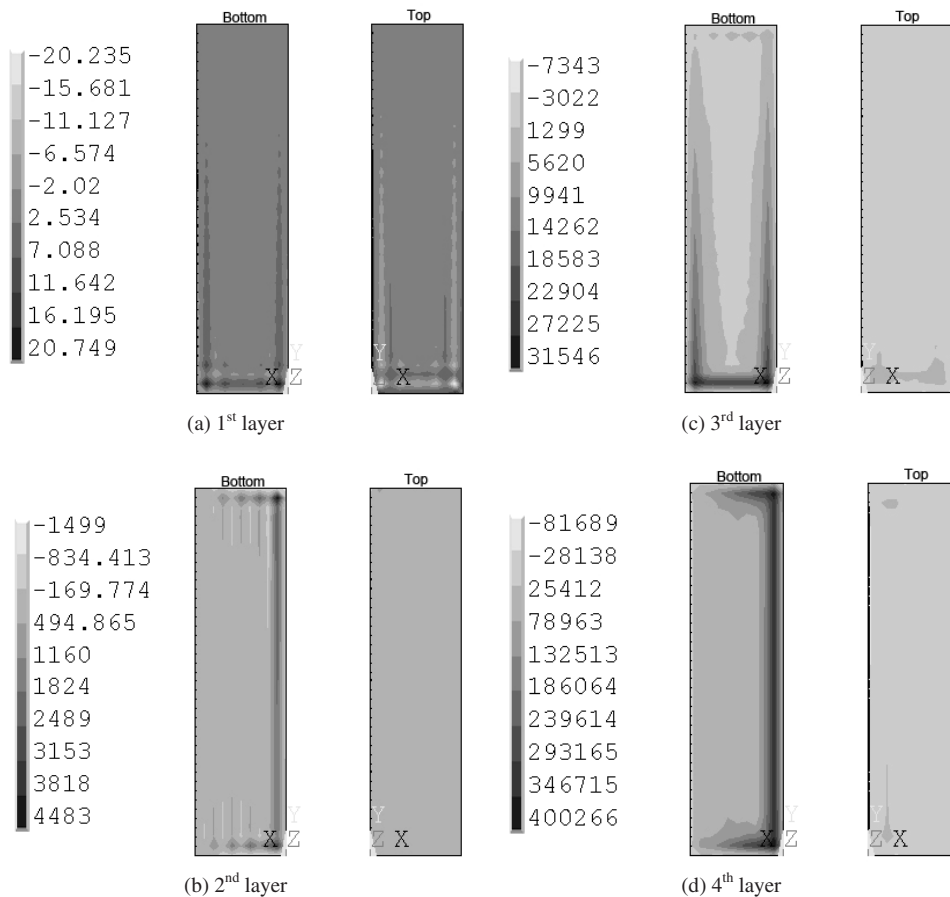


**Fig. 5**  $\sigma_1$  (maximum principal stress) distributions (Pa) after depositions of four consecutive layers: (a) first layer; (b) second layer; (c) third layer; (d) fourth layer

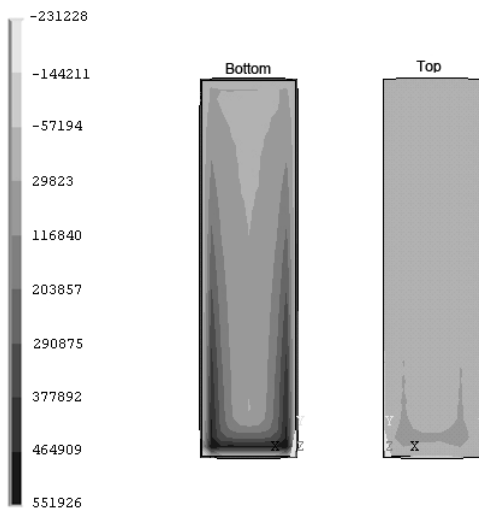
show the largest residual stress. The stress accumulations are caused by the heating-cooling cycles and repeated thermal expansion and contraction. When the very first element of the whole part is activated, it has five effective convection surfaces, and thus the element cools rather quickly. When more elements are activated, the heat from the newly activated element is dissipated into both the semicompleted model and the surrounding air. This makes the cooling process less abrupt and the residual stress generated is less concentrated. Further, since, in the bottom surface, deflections are suppressed, high and concentrated thermal stresses are induced. For the elements on the second and upper layers, their nodes on the bottom plane are not restrained. Therefore, the residual stress is stored towards the bottom of the first layer (i.e. the bottom surface of the part) with a high level of stress gradients as well. Thus, the stress concentration characteristic is aligned along the length side for the long-raster deposition, and the stress-intensity characteristic is aligned along the width side for the short-raster deposition. This triggers a phenomenon showing that the maximum stress zone shifts from the centre of the part

towards the length side and width side for the long-raster pattern and short-raster pattern respectively.

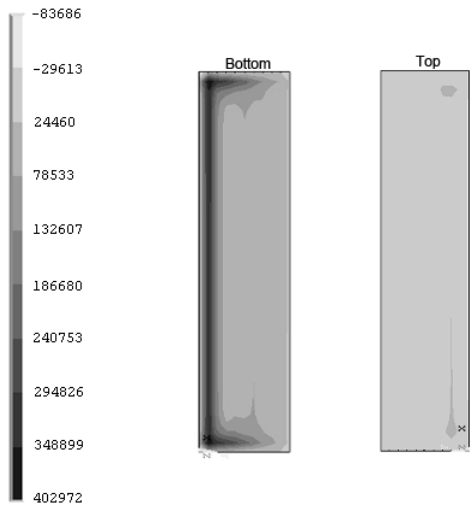
The residual stresses accumulated during the deposition will also cause deflections of the part. The model has been used for deflection simulations for the part by removing displacement constraints at the bottom surfaces of the part. Figure 7 shows one example of deflection simulations ( $z$  direction), for the long-raster tool path. It is shown that the distortion centre shifted towards the length side as the residual stress distribution pattern developed.

### 3.3 Comparisons of distortions of the part

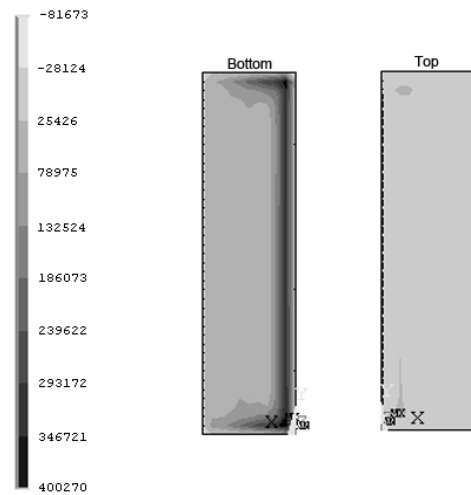
Several prototypes ( $40 \text{ mm} \times 10 \text{ mm} \times 1.016 \text{ mm}$  thin plates) were fabricated using three types of tool-path pattern as corresponding to the simulations, and further measured in dimensions and shape. The fabricated prototypes were mounted on to a metal flat using a seal, with the top surface facing down (Fig. 8). The bottom surfaces of the part were then probed using the coordinate-measuring machine, in the automatic measure mode, for a total of 50



(a) Short-raster pattern



(b) Long-raster pattern



(c) Alternate-raster pattern

**Fig. 6**  $\sigma_1$  (maximum principal stress) distributions (Pa) in finished parts using different tool-path patterns: (a) short-raster pattern; (b) long-raster pattern; (c) alternate-raster pattern

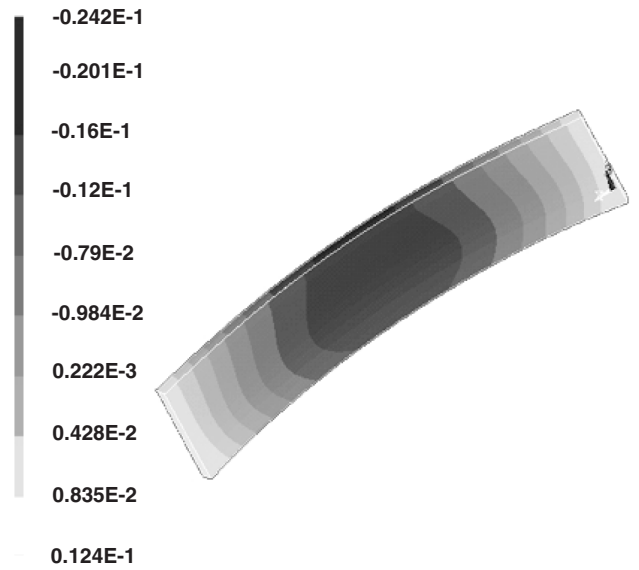


**Fig. 7** An example of simulations of the deflections in a part showing a shift in the distortion centre for a long-raster pattern (units, mm)

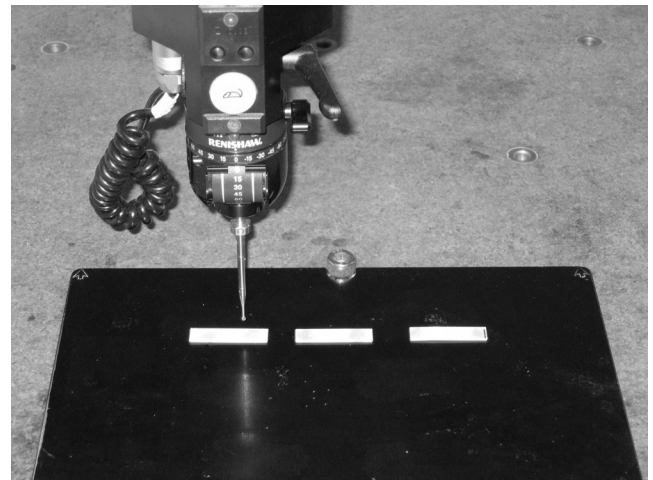


**Fig. 8** A photograph showing the set-up for prototype measurements using a coordinate-measuring machine

equally spaced points. Measured points were used to plot the height contours of the bottom surface for evaluations.

For each tool-path pattern, three samples were duplicated and measured. Figure 9 shows the height-contour plots of the parts fabricated using different tool-path patterns. It can be seen that all measured contours show distortions around the corners, which is consistent with the predictions. In addition, the distortion core does not coincide with the part centre. The distortion characteristics from the experiments show a shift in the distortion centre e.g. the distortion centre of the long-raster part shifts towards the length side, but the distortion centre

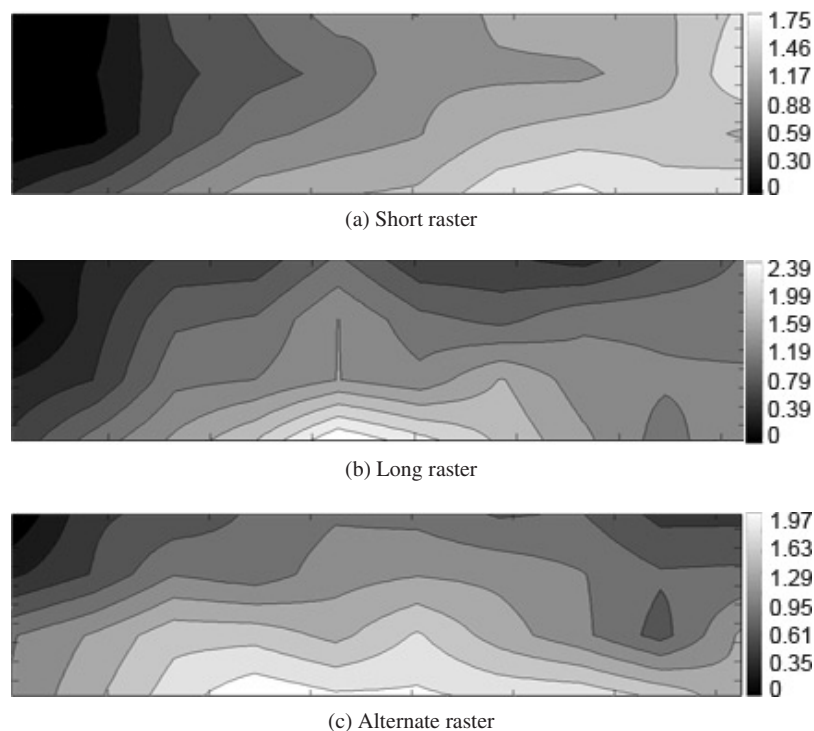


**Fig. 9** Contour plots of prototype bottom surfaces; (a) short-raster pattern; (b) long-raster pattern; (c) alternate-raster pattern (units, mm)

of the short-raster part shifts towards the width side. According to the simulation results (Fig. 6), the residual stresses build up during the deposition process and are altered, both in distribution and in magnitude, by the tool-path pattern and, as a result, the position of the distortion centre is shifted. Thus, the shift in the distortion centre of FDM parts may be due to the change in the residual stress patterns owing to different tool-path patterns. However, the simulated deflections are smaller in magnitude than the experiments, possibly owing to the uncertainty in small part measurements and to the simplified material properties and boundary conditions.

#### 4 CONCLUSIONS

In this study, the FDM process has been simulated using FEA with simplified material properties and boundary conditions. The approach also demonstrates the feasibility of using the element activation function to simulate the filament deposition (in a discretized manner). The simulations of coupled thermomechanical phenomena are used to analyse the stress accumulations during the deposition and resulting distortions of the part. Tool-path effects on the residual stresses and distortion pattern of the part were further investigated. The simulation results show modifications of the residual stress distributions (and also magnitude) as a result of the

tool-path pattern. Prototypes were also fabricated and measured for comparisons of the distortions in the parts. In a similar way, the distortions of the parts observed in the experiments show the same types of modification, i.e. a shift in the distortion centre owing to the tool-path pattern, as in the residual stress distribution. In addition, the simulation results also show that tool-path patterns noticeably affect the deflection of the part as well, because of residual stresses accumulated during the deposition. Thus, it can be suggested that the FDM parts are sensitive to the process parameters including the tool-path pattern and others.

The FEA model adopted in this study resembles one of the most important aspects in FDM, namely continuous changes (addition) in the geometry and boundary conditions, which are different from other LM systems (e.g. SLA and SLS), in which the part is surrounded by raw materials throughout the process. The FEA model proposed in this study is capable of simulations of the residual stress and deflection of the part; however, further work to incorporate comprehensive material behaviour models in different states, with realistic boundary conditions, and with contact bonding is needed to improve the accuracy of prediction. The model may have the potential to assist process optimizations in tool-path planning and part quality. The proposed method may also be used to investigate parts of more complex

geometry, if an adaptive algorithm can be developed to select and activate elements according to the actual tool-path file.

## ACKNOWLEDGEMENT

Helpful discussion with Ken Cooper at Marshall Space Flight Center, National Aeronautics and Space Administration, is gratefully acknowledged.

## REFERENCES

- 1 Qiu, D. and Langrana, N. A. Void eliminating toolpath for extrusion-based multi-material layered manufacturing. *Rapid Prototyping J.*, 2002, **8**(1), 38–45.
- 2 Qiu, D., Langrana, N. A., Danforth, S. C., Safari, A., and Jafari, M. Intelligent toolpath for extrusion-based LM process. *Rapid Prototyping J.*, 2001, **7**(1), 18–24.
- 3 Sabourin, E., Houser, S. A., and Bøhn, J. H. Adaptive slicing using stepwise uniform refinement. *Rapid Prototyping J.*, 1996, **2**(4), 20–26.
- 4 Wool, R. P. and O'Conner, K. M. A theory of crack healing polymers. *J. Appl. Physics*, 1981, **52**(10), 5953–5963.
- 5 Yardimci, M. and Guceri, S. Conceptual framework for the thermal process modelling of fused deposition. *Rapid Prototyping J.*, 1996, **2**(2), 26–31.
- 6 Mahesh, M., Wong, Y. S., Fuh, Y. H., and Loh, H. T. Benchmarking for comparative evaluation of RP systems and processes. *Rapid Prototyping J.*, 2004, **10**(2), 123–135.
- 7 Bugada, G., Cervera, M., Lombera, G., and Onate, E. Numerical analysis of stereolithography processes using the finite element method. *Rapid Prototyping J.*, 1995, **1**(2), 13–23.
- 8 Sonmez, F. O. and Hahn, T. H. Thermomechanical analysis of the laminated object manufacturing (LOM) process. *Rapid Prototyping J.*, 1998, **4**(1), 26–36.
- 9 Dalgarno, K. W., Childs, T. H. C., Rowntree, I., and Rothwell, L. Finite element analysis of curl development in the selective laser sintering process. In Proceedings of the 7th Solid Freeform Fabrication Symposium, 1996, pp. 559–566 (University of Texas, Austin, Texas).
- 10 Chin, R. K., Beuth, J. L., and Amon, C. H. Thermo-mechanical modeling of successive material deposition in layered manufacturing. In Proceedings of the 7th Solid Freeform Fabrication Symposium, 1996, pp. 507–514 (University of Texas, Austin, Texas).
- 11 Chin, R. K., Beuth, J. L., and Amon, C. H. Successive deposition of metals in solid freeform fabrication processes, Part 1: thermomechanical models of layers and droplet columns. *J. Mfg Sci. Engng*, 2001, **123**, 623–631.
- 12 Chin, R. K., Beuth, J. L., and Amon, C. H. Successive deposition of metals in solid freeform fabrication processes, Part 2: thermomechanical models of adjacent droplets. *J. Mfg Sci. Engng*, 2001, **123**, 632–638.
- 13 Nickel, A. H., Barnett, D. M., and Prinz, F. B. Thermal stresses and deposition patterns in layered manufacturing. *Mater. Sci. Engng*, 2001, **A317**, 59–64.
- 14 Ong, R. *Residual stress-induced warping in polymeric parts manufactured by solid freeform fabrication processes*. Master Thesis, Carnegie Mellon University, Pittsburgh, Pennsylvania.
- 15 Finnie, S., Cheng, W., Finnie, I., Drezet, J. M., and Gremaud, M. The computation and measurement of residual stresses in laser deposited layers. *J. Engng Mater. Technol.*, 2003, **125**, 302–308.
- 16 Beuth, J. L. and Narayan, S. H. Residual stress-driven delamination in deposited multi-layers. *Int. J. Solids Structs*, 1996, **33**(1), 65–78.
- 17 Incropera, F. P. and DeWitt, D. P. *Introduction to heat transfer*, 4th edition, 1996 (John Wiley, New York).

